Data-driven Simulation of the Rock Mass Response to Mining: a Status Report

R. J. Durrheim* and D. Labrie**
* Division of Mining Technology, CSIR, South Africa;
** Mining and Mineral Sciences Laboratories, CANMET, Canada

Many mining excavations are situated in overstressed regimes where the rock surrounding any void will fracture and fail, regardless of the rock-breaking method or shape of the excavation. Numerical modelling tools are widely used to determine which mining geometries and sequences will limit the extent of rock failure and to establish the optimum trade-off between the rock engineering ideal and various economic and practical considerations. This series of laboratory experiments seeks to advance efforts to simulate the deformation and failure of the rock mass during mining by integrating physical observations in the numerical modelling process. Simple models were carved from 25 cm sandstone cubes and tri-axially loaded. Sensors and cameras were used to monitor the deformation, acoustic emission and the evolution of damage. The blocks were sliced after completing the tests and the fractures were mapped. Comprehensive data sets were gathered for use in the calibration, evaluation and improvement of numerical modelling codes. Guidelines to address key issues in data-driven modelling are discussed. These include the description of rock properties that vary in space and time; the selection of constitutive equations and failure criteria; and the choice of appropriate numerical modelling codes.

Introduction

Some operating mines and many prospects are situated in stress regimes where the rock surrounding any void will fracture and fail, regardless of the rock-breaking method or the shape of the excavation (Durrheim, 2002; Udd, 2002). It is a challenging task to design and operate a mine in these extreme conditions, especially where the ore body has a complex shape and the rock mass is heterogeneous. The task of the rock engineer is to design the geometry and sequence of excavations so that the risk of rock failure is limited, and to design functional and cost-effective support systems that will control the fractured rock surrounding the excavations (Wagner, 1989). Numerical modelling tools are generally used to evaluate a range of possible mine designs to find the optimum trade-off between the rock engineering ideal and various economic and practical considerations.

The South African SIMRAC and DeepMine Programs have supported efforts to improve the simulation of mining-induced deformation and failure of the rock mass by integrating seismic observations in the numerical modelling process. These techniques have been tested by back-analyzing data sets from seismically active mines (Hoffmann et al., 2001; Spottiswoode, 2001). While promising results have been achieved, there are many opportunities for further improvements. For example:

- Better description of rock properties and rock mass heterogeneity,
- Better mapping of geological structures and discontinuities,
- More complete measurement of rock mass deformation and failure,
- Better measurements of virgin and induced stresses,
- Improved methods to convert the parameters of seismic events to stress or strain changes,
- Formulation of more appropriate constitutive laws and failure criteria, and
- Greater computing power.

Laboratory experiments make it possible to evaluate new modelling concepts and monitoring technologies relatively quickly and cost-effectively as the physical properties of the model can be comprehensively determined, the applied stresses can be precisely controlled, and the deformation adequately measured. While our laboratory models are analogous to mining situations, we have not attempted to create scale models. Our goal is to gather observational data that can be used to calibrate, evaluate and improve existing numerical modelling codes.

The objectives of this study are extremely practical. We aim to develop techniques to incorporate field measurements into numerical modelling codes, thereby improving the match between modelling and reality. We then intend to formulate guidelines that will enable mine operators to allocate their data-gathering resources in the most cost-effective way to enable simulation of the rock mass response to mining. For example, to decide how best to direct resources between exploration drilling, geotechnical mapping, laboratory rock testing, in situ stress measurements and monitoring instrumentation such as micro-seismic systems and strain cells. This will assist the designers and operators of mines excavated in overstressed rock to reduce the risk of rock falls and rockbursts. Furthermore, this work has the potential to improve the efficiency of mining methods that exploit the controlled failure of rock.

Laboratory Experiments

Rock Properties

Simple models were carved from 25 cm cubes of Nepean sandstone, which is a coarse-grained silica rock with a porosity of about 15 per cent. The rock engineering properties were determined by uni-axial, tri-axial and diametral tests on a core drilled from the centre of each cube. Durrheim and Labrie (2004) describe the laboratory experiments performed to gather the basic data used for the numerical modelling exercise. Sensors and cameras were used to monitor the deformation, acoustic emission and the evolution of damage. The blocks were sliced after completing the tests and the fractures were mapped.

Results

'Room and Pillar' Model

A 65 mm high and 30 mm deep groove was carved around the equator of Block #2. A 65 x 65 mm cavity was then cut through the centre of the block to form two rectangular pillars with width:height:length = 1:1:2.7. The major principal stress was applied perpendicular to the bedding of the sandstone. Results of the laboratory tests performed on the core cut from the centre of the block are shown in Figures 1a and 1b.

Six pairs of strain gauges were used to measure the deformation of the model, with three pairs fixed to each pillar. Pre-existing discontinuities were marked with a felt-tipped pen. Load was applied simultaneously and at a constant rate to the top and sides of the block, keeping the vertical and horizontal stress in the immediate floor and roof of each pillar approximately equal (Figure 1c). The areas of the platens, block faces and pillars had been carefully measured in order to calculate the hydraulic line pressures required to achieve the desired loading. Once the average pillar stress (APS) had reached 15.5 MPa the horizontal stress was kept constant, while the vertical load was increased at the same rate as before. A rapid increase in the rates of deformation, damage and acoustic emission occurred 128 minutes after the start of the test indicating that complete failure was imminent, and the test was halted to prevent damage to the AE sensors and camera. The average pillar stress at the termination of the test was 71 MPa. This was far lower than expected as the unconfined compressive strength of the specimen cored from the centre of the block was 133.6 MPa.

The two pillars experienced very different modes of deformation. Pillar 2 experienced vertical compression that increased steadily to reach a value of 0.3 per cent at the end of the test (Figure 1d). Horizontal dilation of the short faces was detected when the APS reached 10 MPa, increasing steadily to reach a value of -0.08 per cent at the end of the test. The centre of the long face initially experienced slight horizontal compression (0.007 per cent) but started to dilate when the APS reached 50 MPa, increasing steadily to -0.025 per cent. Pillar 1 showed a very different pattern: the strains were far smaller, none exceeding 0.01 per cent. The strains measured by the horizontal component gauges were slightly compressional, while the strain measured by the vertical component gauge was mostly dilatational. The reason for the contrasting behaviour became apparent once the block was removed from the press and the presence of a shear fracture running diagonally through Pillar 1 and extending into the roof and floor was noted.

Damage was first observed in the field of view of the camera installed between the pillars about 95 minutes after the start of the test. A notch formed at the intersection of the roof and wall of Pillar 1 and a fracture propagated steadily along this line, periodically ejecting fine dust into the room. There was a dramatic increase in the rate of visible fracturing 128 minutes after the start of the test. The test was halted a minute later after a particularly violent episode of ejections and ruptures (Figure 1e).

The block was sliced parallel to σ_1 and perpendicular to the pillar long-axis. Two very different modes of pillar failure were observed. Extensive crushing had taken place in the core and foundation of Pillar 1. The locus of the most intense crushing was along a line parallel to the intersection of the floor and the outer wall of Pillar 1. A fault zone extended from the bottom edge of the block, through Pillar 1, and "day-lighted" along the roof/wall intersection. In contrast, Pillar 2 exhibited extensile vertical splitting, typical of an unconfined uni-axial compression test.

The eight AE sensors recorded over one million hits. Unfortunately, two of the sensors became detached early in the test, so only a relatively small number of hits were associated and located. Thus, the 40,000 source locations shown on Figure 1f are not representative of the actual distribution of acoustic emissions. Nevertheless, the cumulative acoustic energy emission shows some interesting trends. During the initial 30 minutes of tri-axial loading the rate of acoustic energy release was relatively high. During the next 90 minutes of uni-axial loading the energy release rate was somewhat lower, but quite constant with occasional bursts of emission. Finally, about 10 minutes before the termination of the test, the rate of energy release accelerated indicating that failure was imminent.

This was our first attempt to perform a tri-axial test on a large carved block that had been extensively instrumented, and was a qualified success. An interesting evolution of stress build up, degradation, stress transfer and failure took place. The strain gauges and video camera worked perfectly. Unfortunately, two of the AE sensors became detached. The remaining six sensors provided an informative record of the rate of energy release, but the map of AE locations is incomplete and cannot be used to describe the progression of fracturing. Nevertheless, a rich data set was gathered that provided ample data to use to calibrate and evaluate numerical modelling codes.

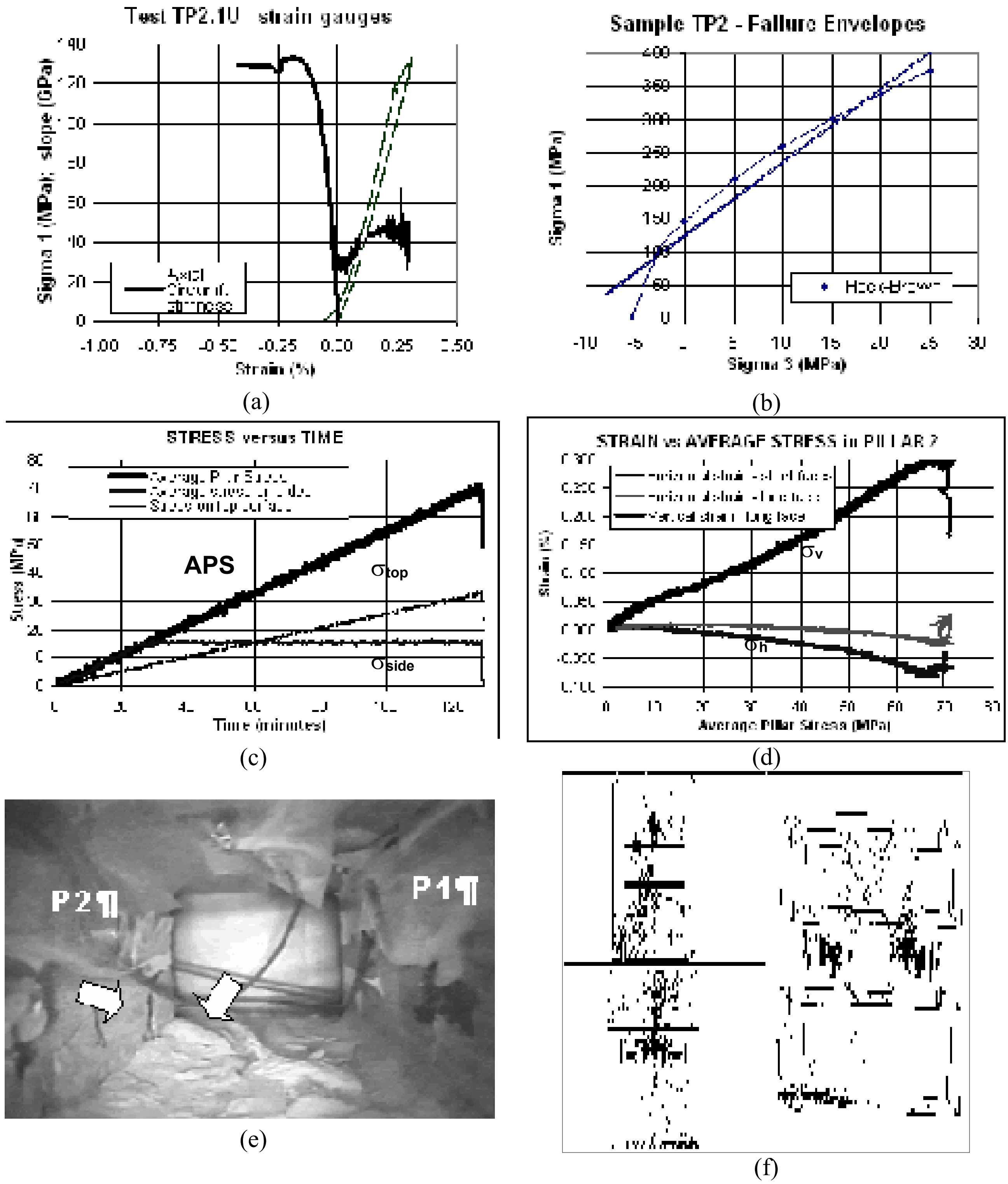

Figure 1. Block #2 tests and experiment (a) Uni-axial test, the axial stiffness was determined by a moving-point regression of the stress-strain curve (b) Hoek-Brown and Mohr-Coulomb failure envelopes (c) Loading of block (d) Deformation of Pillar 2 (e) Video image of the "room" after the test was terminated - note the heave of the floor and slabbing of the Pillar 2 sidewall (f) Acoustic emissions recorded during the experiment - note that the set of source locations is incomplete as two of the eight sensors became detached early in the course of the experiment.

'Micro mine' Model

An 80 mm high and 20 mm deep groove was carved around the equator of Block #3. Care was taken to round the corners of the groove to reduce stress concentrations that might initiate fractures. An 85 x 85 mm cavity was cut through the cube to form a horizontal 'stope' slightly offset from the centre of the block (Figure 2a). A 30 mm diameter 'haulage drift' was bored parallel to the 'stope', and two 30 mm diameter 'cross-cuts' were bored from the outer groove, through the 'haulage drift' into the 'stope', forming 'draw points'. Finally, a 30 mm diameter vertical 'ore pass' was bored through the block, intersecting the 'haulage drift' midway between the 'cross-cuts'.

Five pairs of strain gauges were used to measure the vertical component of deformation. Two pairs were fixed to the 55 mm wide Pillar 1, and three pairs fixed to the 85 mm wide Pillar 2. Although Pillar 2 was wider than Pillar 1, it contained the 'service excavations' and was expected to experience greater degradation and deformation. Two pairs of potentiometers were inserted at the mid- and three-quarter point of the 'stope'. Six AE sensors were inserted in holes drilled in the roof and floor of the cube, deliberately positioned to avoid co-planarity. Another two AE sensors were inserted in holes drilled in the wall of Pillar 2. Video cameras were placed in the 'stope', 'haulage drift' and 'ore pass'.

Load was applied simultaneously and at a constant rate to the top and sides of the block so as to keep the vertical and horizontal stress in the immediate floor and roof of each pillar equal (Figure 2b). Once the average pillar stress (APS) had reached 22 MPa (after 30 minutes loading) the horizontal stress was kept constant, while the vertical load was increased at the same rate as before. Loading and AE monitoring were paused periodically to permit the transmission and recording of seismic pulses through Pillar 2. The test was terminated after 237 minutes when the observed damage and an increase in the AE rate indicated that failure was imminent. The APS was 138 MPa, which is considerably higher than the UCS of the core drilled out to create the 'stope' (83 MPa).

The five pairs of vertical strain gauges showed very similar behaviour (Figure 2c). There was a clear increase in the strain rate (i.e. a softening of the system) when strains were in the range 0.06 to 0.08 per cent and the APS about 56 MPa, with the strain gauge pair located between the 'cross cuts' (2-S4) showing the greatest increase. This occurred about 80 minutes after the start of the test, long before the development of the breakout was observed. The rate of strain on the strain gauge pair between the 'cross cuts' showed another increase when the strain reached 0.22 per cent and the APS reached 130 MPa, about 15 minutes before the test was halted. At the termination of the experiment the greatest strain (0.25 per cent) was measured between the 'cross cuts', while the other four strain gauge pairs showed strains in the range 0.15 to 0.18 per cent.

The two pairs of potentiometers measuring convergence at the mid- and three-quarter point of the stope also showed remarkable consistency (Figure 2d). When the APS reached 22 MPa after 30 minutes of simultaneous horizontal and vertical loading, the measured convergences were in the range 65 - 110 μm. Thereafter the horizontal load was kept constant while the vertical load was increased at the same rate as before. The vertical convergence increased steadily throughout the test, eventually reaching about 500 μm (0.6 per cent). The horizontal components responded in a more complicated way, reversing and decreasing gradually to 40 μm. Then, 15 minutes prior to the end of the test the horizontal convergence at the three-quarter point reversed again. It reached the same maximum value (75 μm) at the termination of the test that it had reached after 30 minutes. This sudden dilation of the pillar coincided with an increase in the pillar strain rate between the 'draw points'.

The first damage was observed about 3 hours after the start of the test when the APS was about 110 MPa. A pair of breakout notches was observed in the 30 mm diameter 'haulage drift', and propagated steadily along the hole until the test was terminated about an hour later (Figure 2e). The 'stope' camera showed the ejection of a slab from the 'draw point' corner at 3h45m. The propagation of a fracture along the floor/wall line was observed at 4 hours. No damage was observed in the 'ore pass', although an accumulation of dust was observed in the 'haulage drift' and on the base platen, probably originating from the breakout developing in the 'haulage drift'.

Over 2,000,000 hits were recorded during the test and some 10,000 sources were located (Figure 2a). The cumulative acoustic energy emission shows similar trends to the 'room and pillar' model. The rate of acoustic energy release was relatively high for the initial 30 minutes of tri-axial loading. During the next 3 hours of uni-axial loading the energy release rate was somewhat lower, although quite constant with occasional bursts. Finally, about 30 minutes before the termination of the test, the rate of energy release accelerated indicating that failure was imminent. The bi-logarithmic relationship between the number of hits as a function of energy and amplitude is fairly linear, consistent with mining-induced and earthquake seismicity (Sellers et al., 2003).

This was our third tri-axial test on a large carved block that had been extensively instrumented, and was a complete success. (The second test was on a 'borehole/tunnel' model that will be described in a separate paper.) The tri-axial loading of the block went according to plan, and the full cycle of stress build-up, local degradation of the rock, stress transfer and failure was monitored. The five pairs of strain gauges, four potentiometers, 8-channel acoustic emission system, two pairs of piezoelectric seismic pulsers/receivers and three video cameras all worked perfectly. An excellent data set was acquired for the calibration and evaluation of numerical modelling codes.

(a)

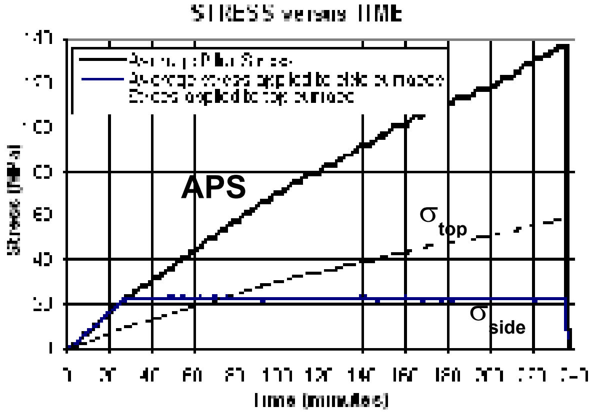

(b)

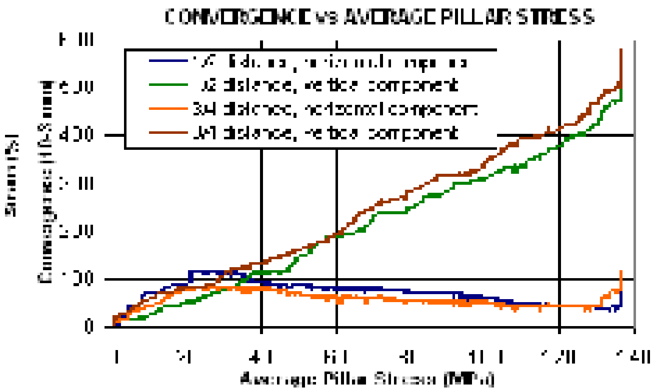

(c)

(d)

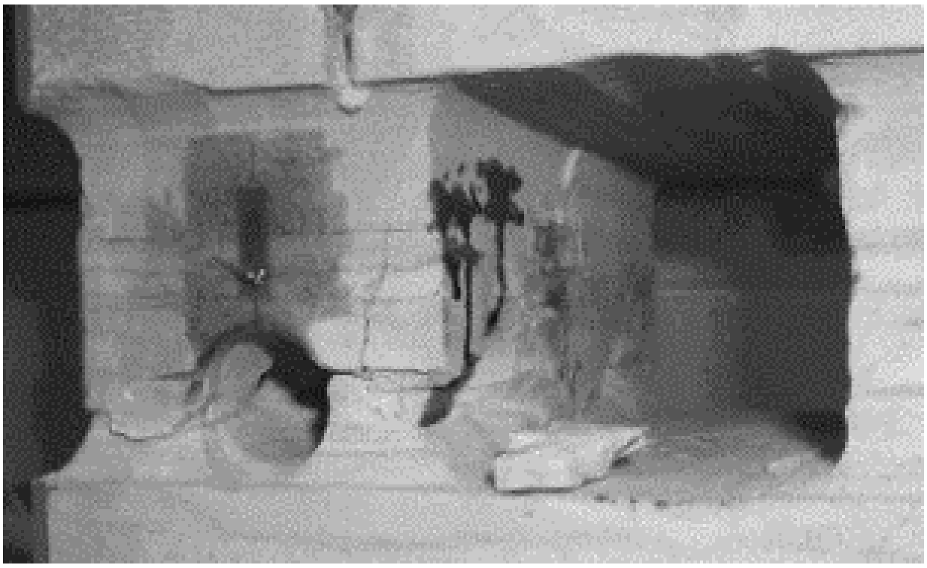

(e)

Figure 2. Block #4 experiment (a) Geometry of model showing acoustic emissions (b) Loading (c) Pillar strain (d) convergence of 'stope' (e) View of damage.

Numerical Modelling

Description of Rock Properties

The intrinsic variability of rock properties may be incorporated into the numerical modelling scheme by means of a statistical distribution of rock properties. Changes in rock properties as the stress field evolves and the rock degrades may be incorporated by schemes to adjust parameters such as rock stiffness and strength.

Another important issue is the relationship between the properties measured in the laboratory and *in situ*. Mohammed et al. (1997) reviewed several thousand papers on numerical modelling and found that only a few hundred mentioned laboratory and rock mass properties. Of those, only some 44 appeared to apply some kind of reduction to account for the differences in strength and stiffness between intact specimens used for laboratory measurements and the *in situ* rock mass. Mohammad et al. (1997) found that compressive strength, on average, was reduced to about a quarter of the laboratory value, and stiffness to about half. They caution that the rock mass property values are not necessarily measured or 'back analysis derived' and could be, in some cases, simply the opinion of the author of the paper and thus reinforce a bias towards conventional wisdom. Mohammed et al. (1997) concluded that the following equation formulated by Mitri et al. (1994) appeared to give the best prediction to the stiffness properties, at least for Rock Mass Ratings above 20:

$$RF = \frac{E_{rm}}{E_{int}} = 0.5\left[1 - \left(cos\left(\pi\ \frac{RMR}{100}\right)\right)\right]$$

where RF is the reduction factor; E_{rm} and E_{int} are the Young's modulus of the rock mass and intact rock, respectively; and R*MR* is the rock mass rating.

In terms of strength properties, Mohammed et al. (1997) recommended the approach of Hoek and Brown (1980), which has subsequently been refined and extended (Hoek and Brown, 1997; Hoek, 1998):

$$\sigma'_1 = \sigma'_3 + \sigma'_3\left(m_b \frac{\sigma'_3}{\sigma_{ci}} + s\right)^a$$

where σ'_1 and σ'_3 are the maximum and minimum effective stresses at failure, respectively; m_b is the value of the Hoek-Brown constant m for the rock mass; s and a are constants which depend on the characteristics of the rock mass, and σ_{ci} is the uniaxial compressive strength of the intact rock pieces. For intact rock, s =1 and a = 0.5. Hoek and Brown (1997) recommend that the values of the m_i be determined by a statistical analysis of the results of a set of triaxial tests on carefully prepared core samples. When using the Hoek-Brown criterion to estimate the strength of jointed rock masses, the Geological Strength Index (GSI) is used to estimate the rock mass parameters m_b, s and a:

$$m_b = m_i \exp\left(\frac{GSI - 100}{28}\right) \text{ and } s = \exp\left(\frac{GSI - 100}{9}\right)$$

For rocks of reasonable quality (GSI>25), a = 0.5.

Constitutive Equations and Failure Criteria

A stress-strain curve for a uniaxial compression test can be divided into four segments from the onset of loading until peak strength (UCS) is reached: (i) crack closure, (ii) elastic deformation, (iii) stable crack growth, and (iv) unstable cracking associated with permanent axial deformation. Only the second stage is strictly linear elastic. Stable cracking typically initiates at uniaxial loads between 0.3 and 0.5 UCS in low-porosity rocks. The stress at which unstable cracking commences is a good indication of the long-term strength of a rock. It is typically initiated between 0.7 and 0.8 UCS, where a reversal in slope of the volumetric strain curve indicates that the rock is experiencing macro-scale dilation (Martin, 1997). Nevertheless, when used with care and insight, linear elastic codes can give very useful results. A useful technique to analyse the linearity of the stress-strain curve is to compute a moving point linear regression (Eberhart et al., 1998; see Figure 1a).

Numerous failure criteria have been proposed. Several reviews and comparisons have recently been published. Colmenares and Zoback (2002) examined seven different failure criteria by comparing them to published poly-axial (σ_1>σ_2>σ_3) test data for five different rock types (dolomite, sandstone, limestone, shale and amphibolite) at a variety a stress states. The poly-axial criteria Modified Wiebols-Cook and Modified Lade achieved a good fit to most of the test data, especially for those rocks with a highly σ_2-dependent behaviour. However, the failure of some rock types is scarcely affected by σ_2 and the Mohr-Coulomb and Hoek-Brown criteria fit the test data equally well, or even better, than the more complicated poly-axial criteria. In general, the Circumscribed and Inscribed Drucker-Prager failure criteria did not accurately indicate the value of σ_1 at failure.

Choice of Numerical Modelling Code

There are numerous factors to be considered when choosing a numerical modelling code, e.g. ease of data input, speed of computation, size and detail of model, nature of rock mass (continuity, heterogeneity etc), geometry of the excavations, desired accuracy of solution. Most commonly used stress analysis codes used for mine design are based on either the boundary element or finite elements methods, each having merits and limitations. Boundary element codes are able to model complex mine geometries excavated in homogeneous and elastic rock very efficiently, but experience difficulty handling inhomogeneous rock masses. Finite element codes, on the other hand, easily incorporate inhomogeneities but require considerably more disk space and running time, thereby limiting the number of elements that can be used to construct a model. Ideally, the practitioner should have a range of codes available and sufficient insight to choose the code(s) and input parameters most suitable to the job at hand.

The discontinuous nature of the rock mass is sometimes fundamental to the problem being addressed. For example, when simulating caving, blasting, fault-controlled deformation or the behaviour of highly fractured rock, treating the rock mass as a continuum could lead to misleading conclusions. The basic difference between discrete element methods and continuum-based methods is that the contact patterns between components of the system are continuously changing with the deformation process for the former, but are fixed for the latter. This introduces a whole range of challenges, e.g. space sub-division and identification of block system topology, representation of block deformation, algorithms for contact detection, constitutive equations for rock blocks and fractures (Jing, 2003).

Conclusions

The long-term objective of this project is the development of better strategies and tools to simulate the response of an overstressed rock mass to mining by gathering appropriate rock property, deformation and damage data and using it to calibrate, evaluate and improve stress analysis codes. This paper describes the first stage of this project, *viz.* the development of techniques to monitor the deformation, degradation, stress transfer and failure of tri-axially loaded rock models. This will make it possible to evaluate new concepts and techniques relatively quickly and cost-effectively. The tests carried out on the large (25 cm cubes) 'room and pillar' and 'micro-mine' models carved from Nepean sandstone document the experience we have gained in monitoring the response of rock models while loaded to the point of failure.

Guidelines to address key issues in data-driven modelling are discussed. These include the description of rock properties that vary in space and time; the selection of constitutive equations and failure criteria; and the choice of numerical modelling codes.

For the next series of tests we plan to study and compare the response of 'room and pillar', 'borehole/tunnel' and 'micro-mine' models carved from Barre granite, Cairnside sandstone and Matagami sulphide ore. We also plan to introduce a couple of new models, e.g. a 'tabular stope' and a 'discontinuous rock mass'. Once we have validated the numerical simulation techniques on laboratory data, we intend to undertake *in situ* mine studies.

Acknowledgements

The authors gratefully acknowledge the support given to this international collaborative research project by Dr Güner Gürtunca and Mr Roy Sage, at the time directors of CSIR Miningtek and CANMET Mining and Mineral Sciences Laboratories, respectively. The laboratory work was carried out at CANMET's Bells Corners Complex in Ottawa, where Ted Andersen, Blain Conlon, Ken Judge and Glenn Poirier provided outstanding technical support. Other CANMET researchers that contributed to the project are Jane Alcott, Dr Marc Betournay, Russell Boyle, Chantale Doucet, Dr Véronique Falmagne, Bernie Gorski, Dr Gary Li, Michel Plouffe and Dr Shahriar Talebi. The CSIR researchers that contributed are Drs Milton Kataka, Lindsay Linzer, Ewan Sellers and Steve Spottiswoode.

References

COLMENARES, L.B. & ZOBACK, M.D. A statistical evaluation of intact rock failure criteria constrained by poly-axial test data for five different rocks. *Int. J. Rock Mech. Min. Sci. 39:* pp. 695-729, 2002.

DURRHEIM, R.J. Stability and support of tunnels and ore-passes in ultra-deep Witwatersrand gold mines: findings of the DEEPMINE Research Programme. *Proc. 2nd Int. Seminar on Surface Support Liners*, South African Institute of Mining and Metallurgy, section 10, pp. 6, 2002.

DURRHEIM, R.J. & LABRIE, D. Data–driven simulation of the rock mass response to mining (Part 1): Laboratory experiments using Nepean sandstone models. In *Proc. 2nd Int. Seminar on Deep and High Stress Mining*, South African Institute of Mining and Metallurgy Symposium Series, 2004

HOEK, E. & BROWN, E.T. *Underground Excavations in Rock*, Inst. Min. Metall., London, 527 pages, 1980.

HOEK, E. & BROWN, E.T. Practical estimates of rock mass strength. *Int. J. Rock Mech. Min. Sci. 34:* pp. 1165-1186, 1997.

HOEK, E. Reliability of Hoek-Brown estimates of rock mass properties and their impact on design. *Int. J. Rock Mech. Min. Sci. 35:* pp. 63-68, 1998.

HOFFMANN, G., SEWJEE, R. & VAN ASWEGEN, G., First steps in the integration of numerical modelling and seismic monitoring. In *Proc. 5th Int. Symposium on Rockbursts and Seismicity in Mines*, (eds. G.A. van Aswegen, R.J. Durrheim and D.W. Ortlepp), South African Institute of Mining and Metallurgy, pp. 397-404, 2001.

JING, L. A review of techniques, advances and outstanding issues in numerical modelling for rock mechanics and rock engineering. *Int. J. Rock Mech. Min. Sci. 40:* pp. 283-353, 2003.

MARTIN, C.D. Seventeenth Canadian Geotechnical Colloquium: The effect of cohesion loss and stress path on brittle rock strength. *Can. Geotech. J. 34:* pp. 698-725, 1997.

MITRI, H.S., EDRISSI, R. & HENNING, J. Finite element modelling of cable-bolted stopes in hard rock underground mines. *Presented at the SME Annual Meeting*, Albuquerque, New Mexico, 14-17 February, 1994, Paper Number 94-116, 1994.

MOHAMMAD, N. REDDISH, D.J. & STACE, L.R. The relation between in situ and laboratory rock properties used in numerical modelling. *Int. J. Rock Mech. Min. Sci. 34:* pp. 289-297, 1997.

SELLERS, E., KATAKA, M.O. & LINZER, L. Source parameters of acoustic emission sources and scaling with mining induced seismicity. *J. Geophys. Res., 108*, pp. ESE 7-1 – 7-16, 2003.

SPOTTISWOODE, S.M. Keynote address: Synthetic seismicity mimics observed seismicity in deep tabular mines. In *Proc. 5th Int. Symposium on Rockbursts and Seismicity in Mines*, (eds. G.A. van Aswegen, R.J. Durrheim and D.W. Ortlepp), South African Institute of Mining and Metallurgy, pp. 371-378, 2001.

UDD, J.E. Deep mining in Canada – the challenges and opportunities. In *Proc. 1st Int. Seminar on Deep and High Stress Mining*, Australian Centre for Geomechanics, Perth Australia, Section 3, 22 p., 2002

WAGNER, H. Underground openings in overstressed rock. *Proc. 6th Int. Rock Mechanics Congress*, Balkema; Rotterdam: 1443-1456, 1989.